Science Advances
AAAS

Supplementary Materials for

Engineered neutrophil-derived exosome-like vesicles for targeted cancer therapy

Jiahui Zhang, Cheng Ji, Hongbo Zhang, Hui Shi, Fei Mao, Hui Qian, Wenrong Xu, Dongqing Wang, Jianming Pan, Xinjian Fang*, Hélder A. Santos*, Xu Zhang*

*Corresponding author. Email: xuzhang@ujs.edu.cn (X.Z.); h.a.santos@umcg.nl (H.A.S.); lygfxj@126.com (X.F.)

Published 12 January 2022, *Sci. Adv.* **8**, eabj8207 (2022)
DOI: 10.1126/sciadv.abj8207

This PDF file includes:

Figs. S1 to S37

Supplementary Materials

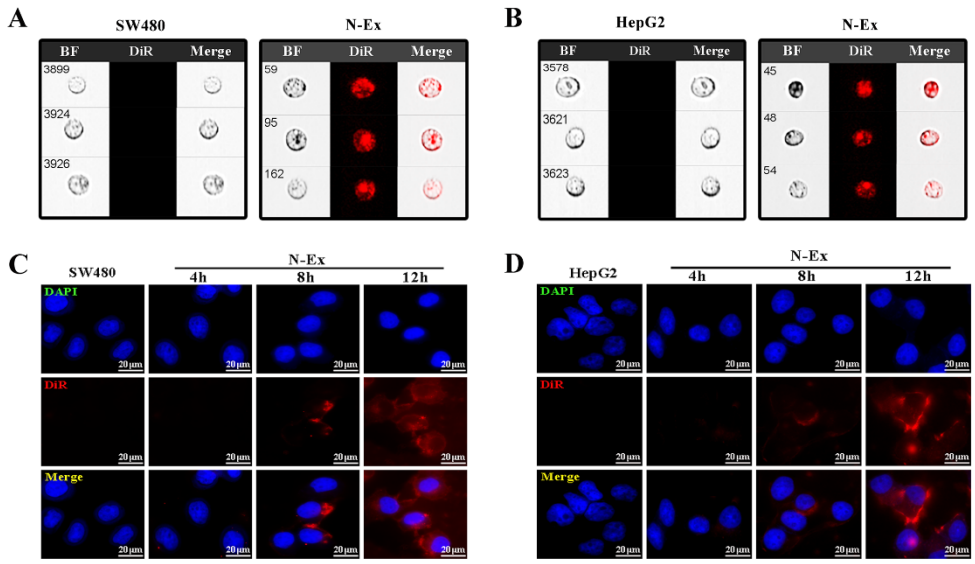

Fig. S1. The uptake of N-Ex by tumor cells.

Cellular uptake of DiR-labeled N-Ex (red fluorescence) by tumor cells (SW480 and HepG2) was detected by imaging flow cytometry (**A and B**) and fluorescence confocal laser microscopy (**C and D**). Scale bar, 20 μm.

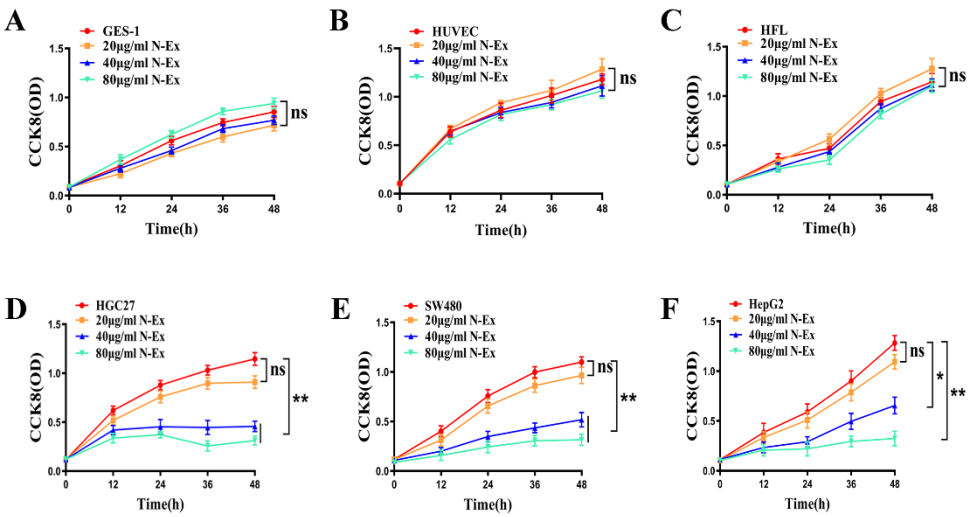

Fig. S2. Cytotoxic effect of N-Ex on normal and tumor cells.

(**A to C**) Cell viability of GES-1, HUVEC, and HFL cells treated with different doses of N-Ex (20, 40, 80 μg/mL) was determined by CCK-8 assay. (**D to F**) Cytotoxic effect of N-Ex (20, 40, 80 μg/mL) on HGC27, SW480, and HepG2 cells. Data are shown as mean ± SD and analyzed by One-way ANOVA. ns: no significant change, **P*<0.05 and ***P*<0.01.

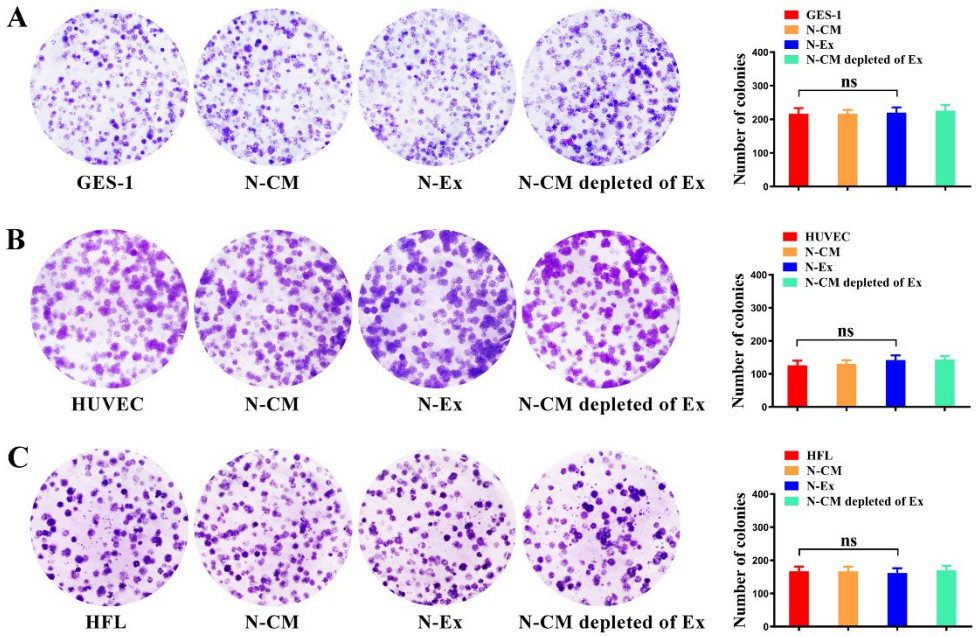

Fig. S3. Cell colony formation ability of normal cells treated with N-Ex.

(**A to C**) Cell colony formation assays for GES-1, HUVEC, and HFL cells treated with N-CM, N-Ex (40 μg/mL), and N-CM depleted of Ex for 24 h. Data are shown as mean ± SD and analyzed by One-way ANOVA. ns: no significant change.

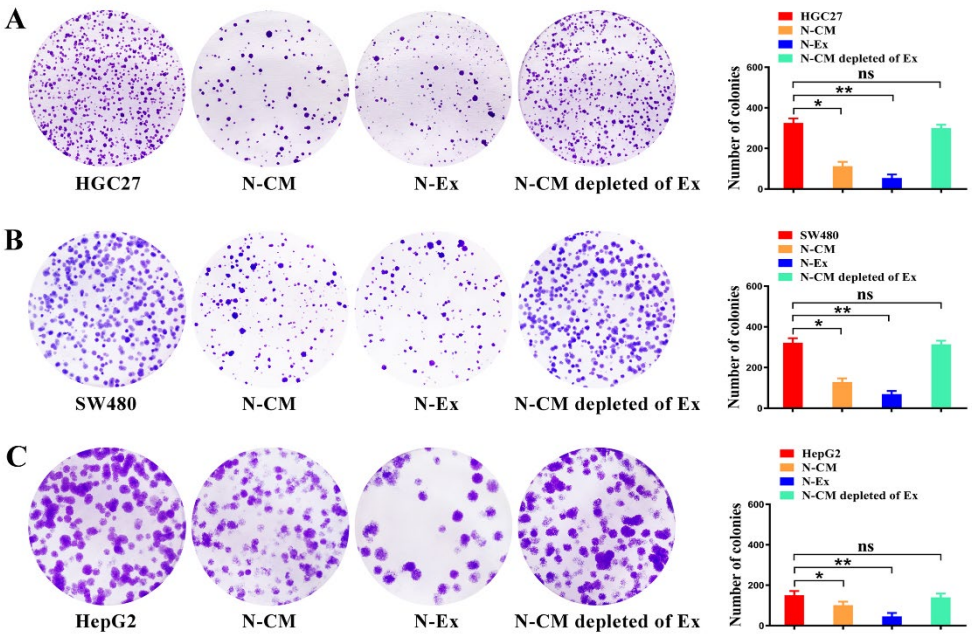

Fig. S4. Effect of N-Ex on the colony formation ability of tumor cells.

(**A to C**) Cell colony formation assays for HGC27, SW480, and HepG2 cells treated with N-CM, N-Ex (40 μg/mL) and N-CM depleted of Ex for 24 h. Data are shown as mean ± SD and analyzed by One-way ANOVA. ns: no significant change, **P*<0.05 and ***P*<0.01.

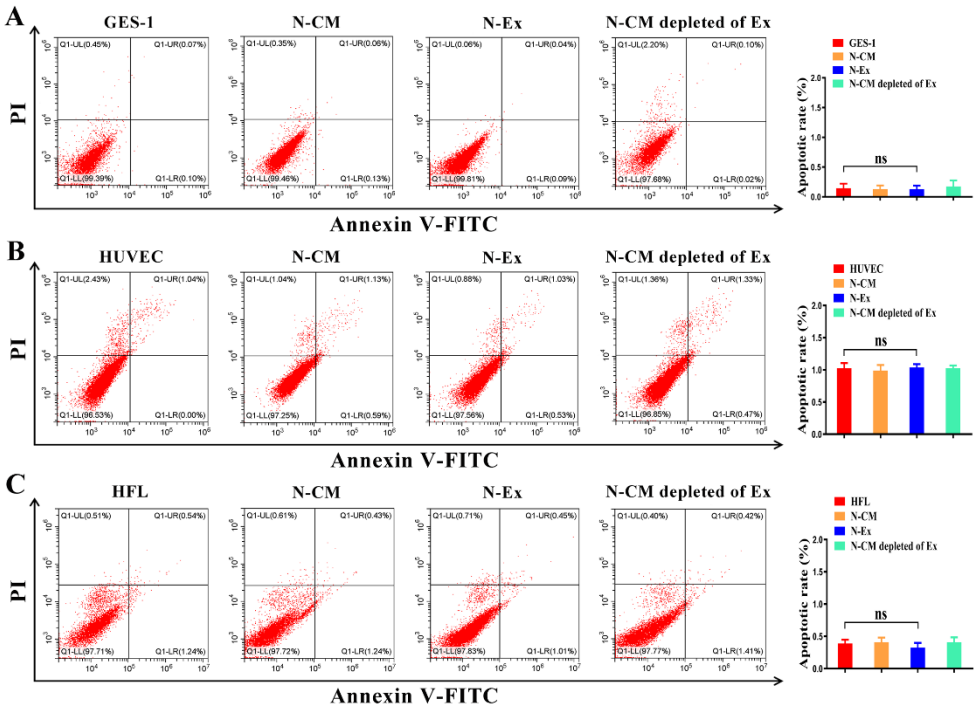

Fig. S5. Cell apoptosis in normal cells treated with N-Ex.

(**A to C**) GES-1, HUVEC, and HFL cells were treated with N-CM, N-Ex (40 μg/mL) and N-CM depleted of Ex for 24 h, collected and stained with Annexin V-FITC and propidium iodide and then analyzed by flow cytometry. Data are shown as mean ± SD and analyzed by One-way ANOVA. ns: no significant change.

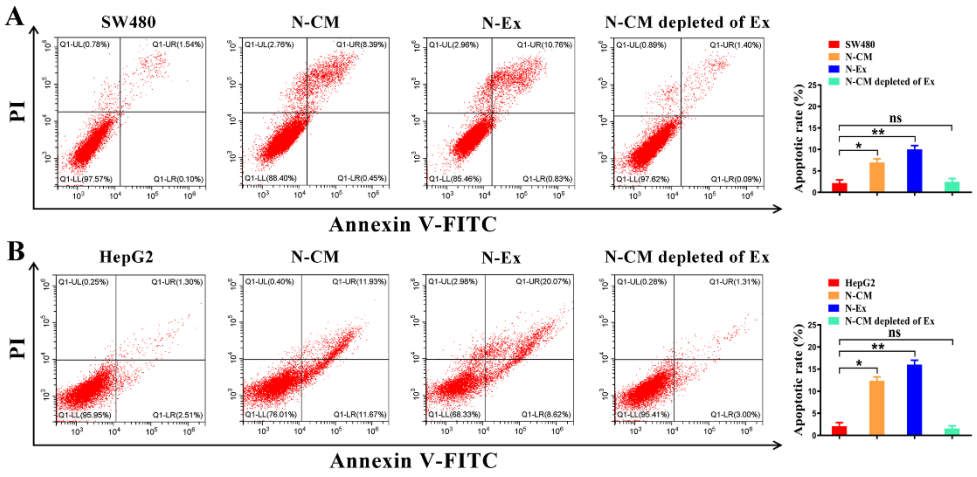

Fig. S6. Effect of N-Ex on tumor cell apoptosis.

(**A and B**) The apoptotic rate of tumor cells (SW480 and HepG2) treated with N-Ex (40 μg/mL) was analyzed by the flow cytometry. Data are expressed as mean ± SD and analyzed by One-way ANOVA. ns: no significant change, **P*< 0.05, ***P*< 0.01.

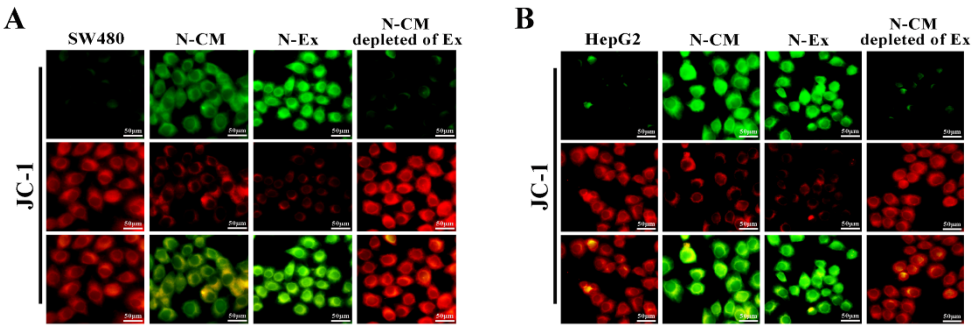

Fig. S7. Mitochondrial membrane potential of tumor cells treated with N-Ex.

(**A and B**) The effects of N-CM, N-Ex (40 μg/mL), and N-CM depleted of Ex on the mitochondrial membrane potential of tumor cells (SW480 and HepG2) were examined by JC-1 staining at 24 h after treatment. The experiments were performed in triplicate and the representative images were shown. Scale bar, 50 μm.

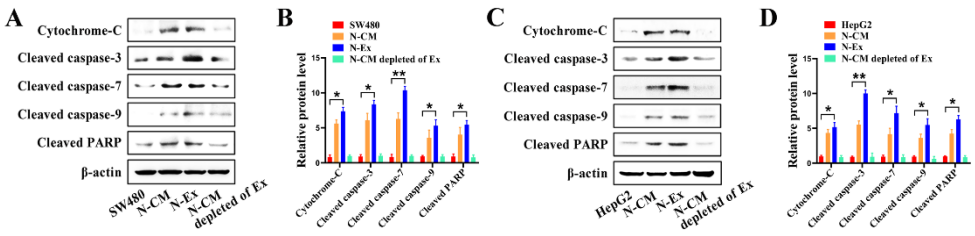

Fig. S8. Expression of proteins in apoptosis signaling pathway in tumor cells treated with N-Ex.

(**A and B**) SW480 and (**C and D**) HepG2 cells were treated with N-CM, N-Ex (40 μg/mL), and N-CM depleted of Ex for 24 h. The expression of proteins in apoptosis signaling pathway including cytochrome c, cleaved caspase-3, cleaved caspase-7, cleaved caspase-9, and cleaved PARP was determined by Western blot. The experiments were performed in triplicate. Data are expressed as mean ± SD and analyzed by One-way ANOVA. ns: no significant change, **P*<0.05 and ***P*<0.01.

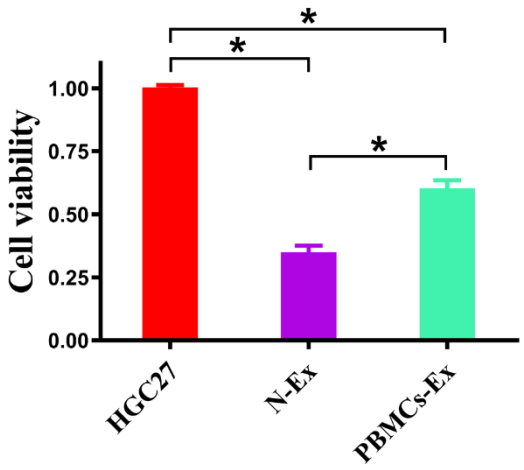

Fig. S9. The anti-tumor efficacy of N-Ex and PBMCs-Ex.

Cell viability of HGC27 cells treated with N-Ex (40 μg/mL) and PBMCs-Ex (40 μg/mL) for 24 h was evaluated by CCK-8 assay. Data are expressed as mean ± SD and analyzed by One-way ANOVA. ns: no significant change, *P< 0.05.

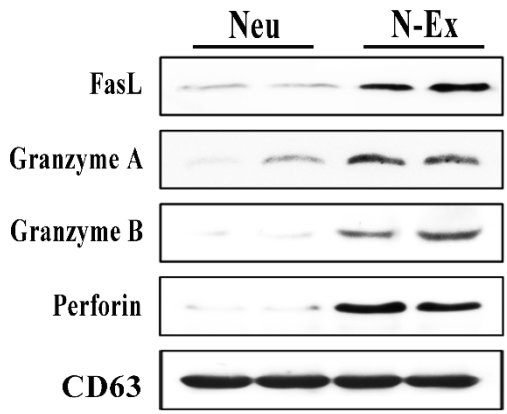

Fig. S10. Expression of apoptosis-inducing proteins in N-Ex.

The expression of FasL, Granzyme A, Granzyme B, and perforin in N-Ex was determined by Western blot. CD63 was used as the loading control.

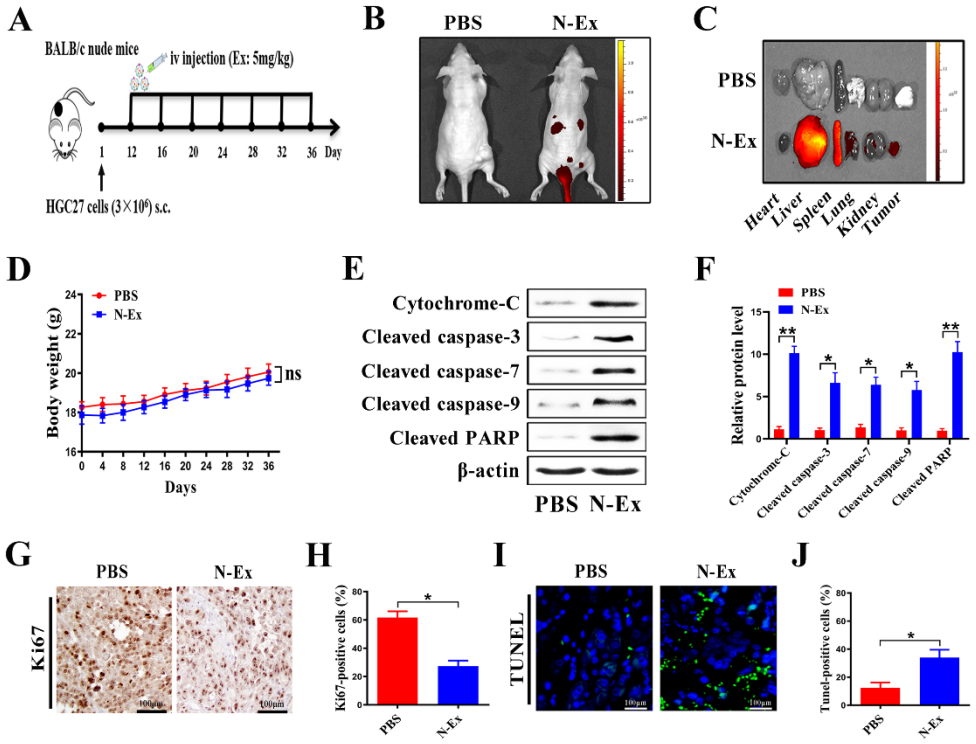

Fig. S11. Therapeutic effect of intravenously injected N-Ex on subcutaneous xenograft tumor in BALB/c nude mice.

(**A**) Schematic diagram showing the procedure for intravenous injection of N-Ex (5 mg/kg of body weight; 100 μL) on a subcutaneous xenograft tumor model (n=5 per group). (**B and C**) The fluorescence signals of DiR-labeled N-Ex in major organs and tumors of BALB/c nude mice were detected by IVIS imaging system at three days after last injection (day 39). (**D**) Body weights of BALB/c nude mice in PBS and N-Ex-treated groups. (**E and F**) Western blot assays for the expression of apoptosis signaling pathway proteins in tumors from N-Ex-treated mice. (**G and H**) Ki-67 staining of tumors from N-Ex-treated mice. Scale bar, 100 μm. (**I and J**) TUNEL staining for apoptotic cells in tumors from N-Ex-treated mice. The quantification of apoptotic cells per filed was presented. Scale bar, 100 μm. Data are representative of at least three independent experiments and analyzed by Student's *t*-test. ns: no significant change, **P*<0.05 ***P*<0.01.

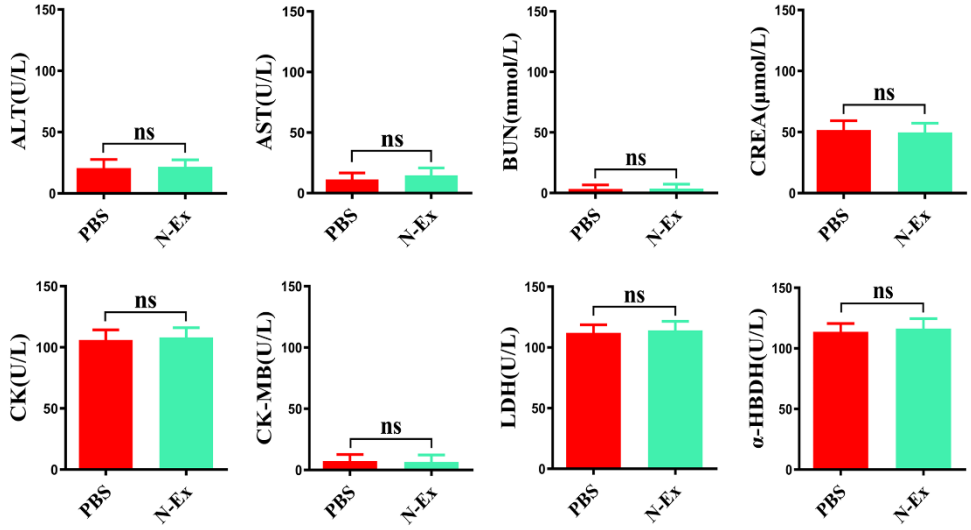

Fig. S12. Liver, kidney, and heart functions of BALB/c nude mice treated with N-Ex.

Liver (ALT and AST), kidney (BUN and CREA), and heart (CK, CK-MB, LDH and α-HBDH) functions of BALB/c nude mice treated with N-Ex (5 mg/kg of body weight; 100 μL) were determined by blood biochemical tests. Mouse blood samples were collected at three days after the last injection. Data are expressed as mean ± SD and analyzed by Student's *t*-test. ns: no significant change.

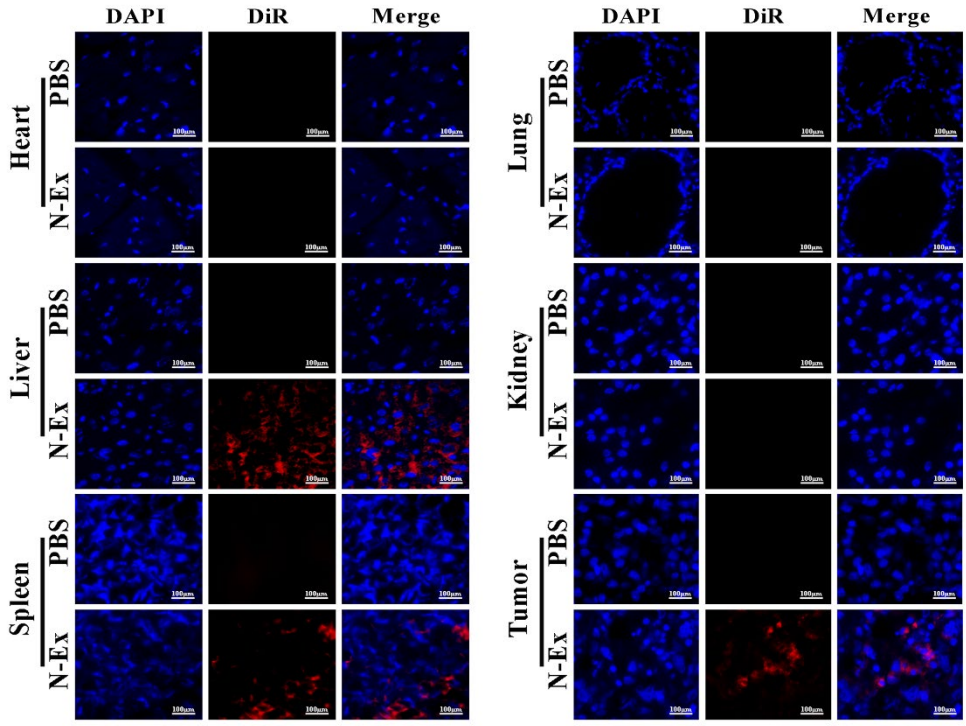

Fig. S13. Representative fluorescence images of N-Ex in tumors and major organs.

The major organs and tumors of BALB/c nude mice were collected at three days after the last injection (day 39). The accumulation of DiR-labeled N-Ex in tumors and major organs was evaluated by fluorescence confocal laser microscopy. Cell nuclei were stained with DAPI. The red color indicated DiR-labeled N-Ex. Scale bar, 100 μm.

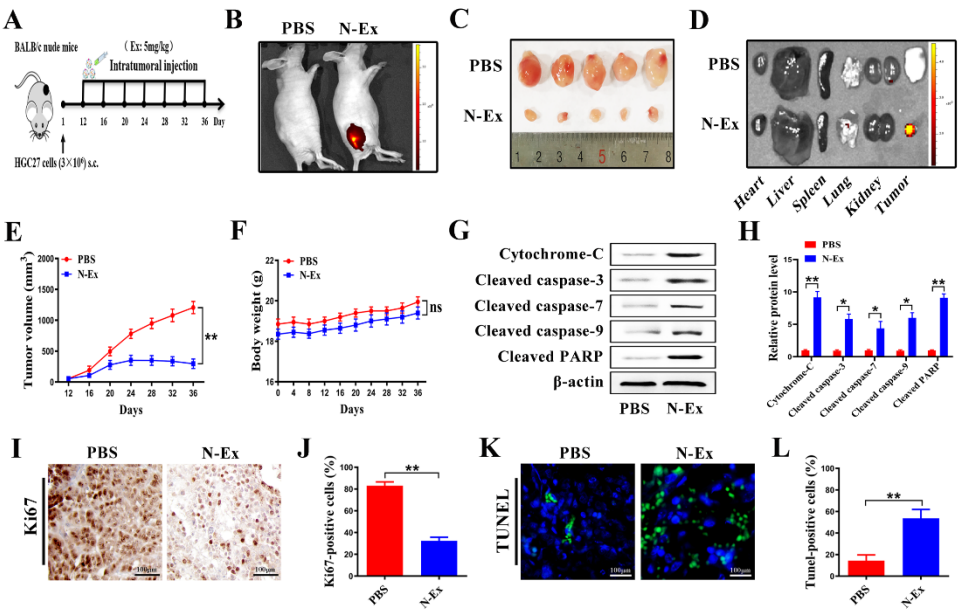

Fig. S14. Intratumoral injection of N-Ex for tumor therapy.

(**A**) Schematic diagram showing the procedure for intratumoral injection of N-Ex (5 mg/kg of body weight; 100 μL) for 7 cycles on a subcutaneous xenograft tumor model (n=5 per group). (**B**) Fluorescent signals of injected N-Ex in mouse tumor. (**C**) Images of xenograft tumors from the BALB/c nude mice (n=5). (**D**) Fluorescent images of tumors and major organs at three days after last injection (day 39). (**E**) Tumor growth curves of N-Ex-treated mice. (**F**) Body weights of mice in N-Ex-treated group. (**G and H**) The expression of apoptosis signaling pathway proteins in tumors from N-Ex-treated group was determined by Western blot. (**I and J**) Ki-67 staining of tumor tissues from control and N-Ex-treated mice. (**K and L**) TUNEL staining for cell apoptosis in tumor tissues from control and N-Ex-treated mice. Scale bar, 100 μm. Data are expressed as mean ± SD and analyzed by Student's *t*-test. ns: no significant change, **P*<0.05 ***P*<0.01.

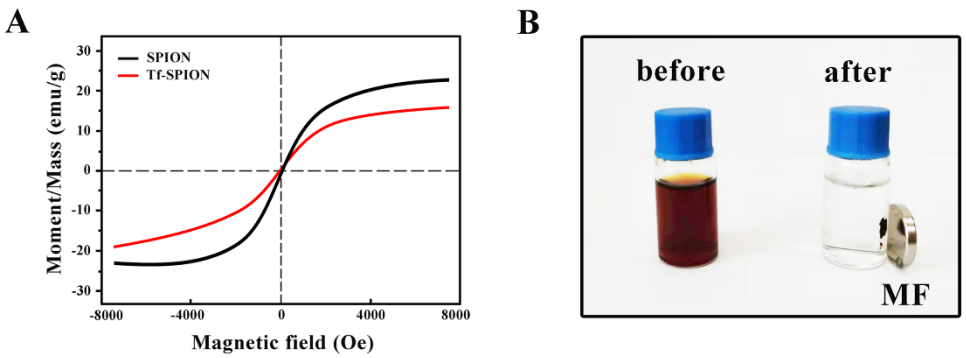

Fig. S15. Magnetic behaviors of SPION *in vitro*.

(**A**) The magnetic hysteresis loops of SPION and Tf-SPION. (**B**) Magnetism response of Tf-SPION. The dispersed Tf-SPION rapidly adhered to the wall of vials when an external MF was applied.

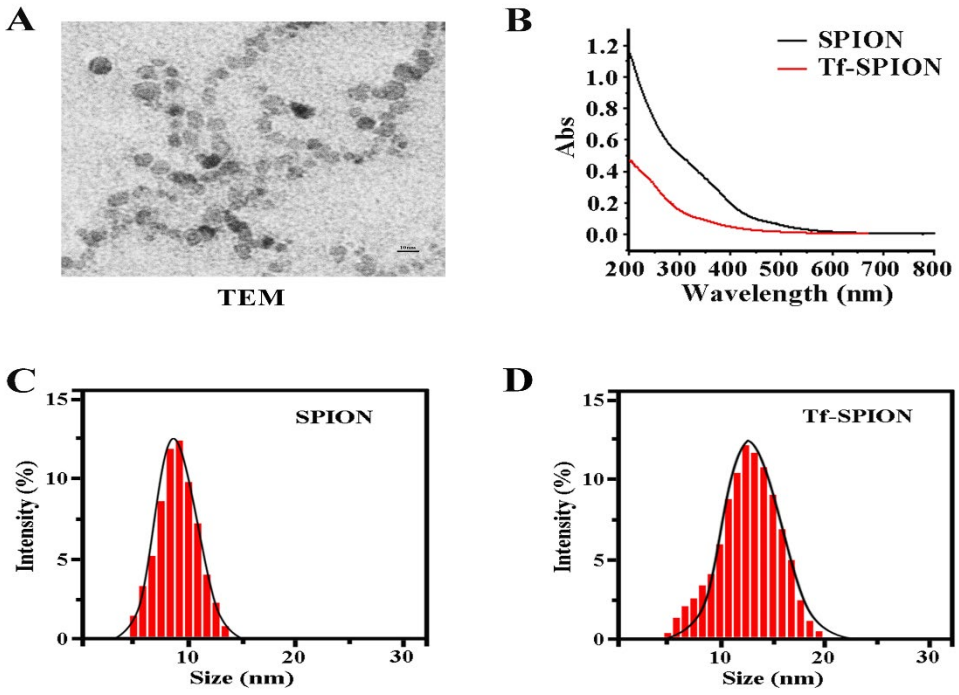

Fig. S16. Characteristics of Tf-SPION.

(**A**) TEM images of Tf-SPION. Scale bar, 10 nm. (**B**) UV spectrophotometric analysis of SPION and Tf-SPION. (**C and D**) Size distribution of SPION and Tf-SPION was measured by DLS.

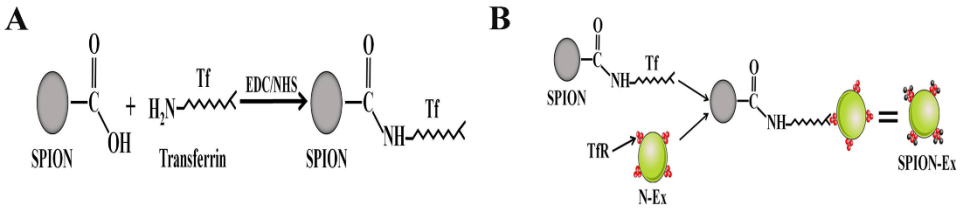

Fig. S17. Generation of Tf-SPION for N-Ex isolation.

(**A**) The anchoring of holo-Tf to SPION. (**B**) Incubation of Tf-SPION with N-Ex to form SPION-Ex through Tf-TfR interaction.

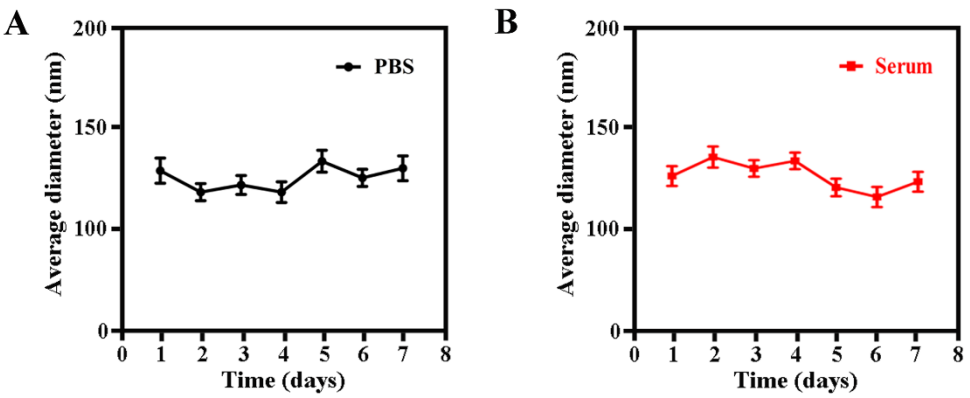

Fig. S18. The stability of SPION-Ex.

(**A to B**) The size distribution of SPION-Ex in PBS (A) and serum (B) was determined by dynamic light scattering.

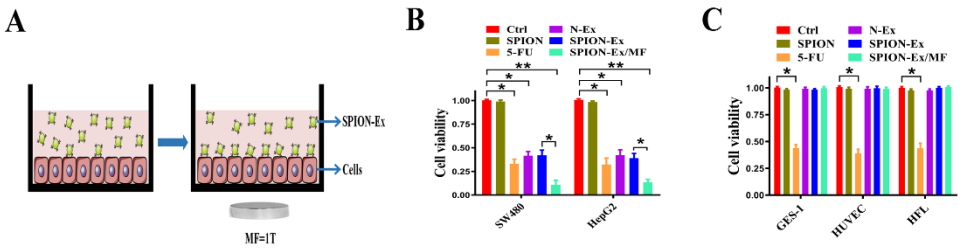

Fig. S19. Effect of SPION-Ex on the viability of tumor and normal cells.

(**A**) Schematic diagram showing the treatment of tumor and normal cells with SPION-Ex under an external MF. (**B**) CCK-8 assay for the viability of SW480 and HepG2 cells treated with SPION (100 μg/mL), 5-FU (30 μg/mL), N-Ex, SPION-Ex (40 μg/mL) with or without MF for 24 h. (**C**) Cytotoxic effect of SPION (100 μg/mL), 5-FU (30 μg/mL), N-Ex, SPION-Ex (40 μg/mL) with or without MF on GES-1, HUVEC, and HFL cells at 24 h after treatment was determined by CCK-8 assay. Data are expressed as mean ± SD and analyzed by one-way ANOVA. ns: no significant change, **P*< 0.05, ***P*< 0.01.

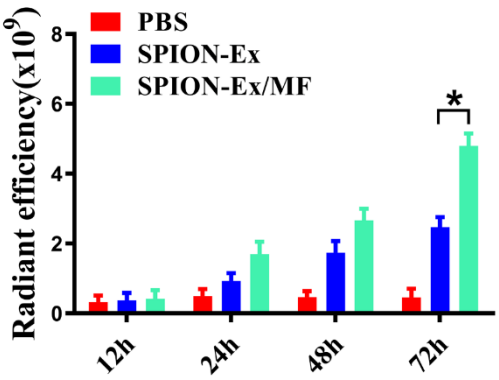

Fig. S20. Fluorescence intensity of DiR-labeled SPION-Ex *in vivo*.

Quantitative analyses of fluorescence intensity of DiR-labeled SPION-Ex in the tumors of BALB/c nude mice at 12, 24, 48, 72 h after intravenous injection (with or without MF). Data are expressed as mean ± SD and analyzed by one-way ANOVA. ns: no significant change, *P< 0.05 and **P< 0.01.

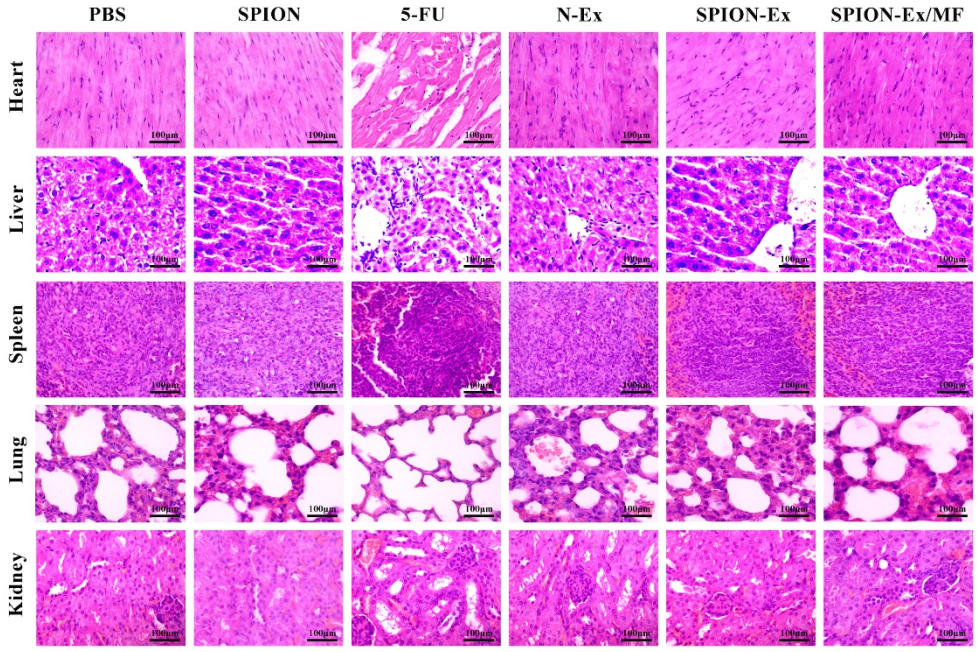

Fig. S21. Histological analyses of major organs in different groups.

BALB/c nude mice were sacrificed at three days after last injection of SPION-Ex (day 39) and the major organs of mice in each group including liver, spleen, heart, lung, and kidney were collected for H&E staining. Scale bar, 100 μm.

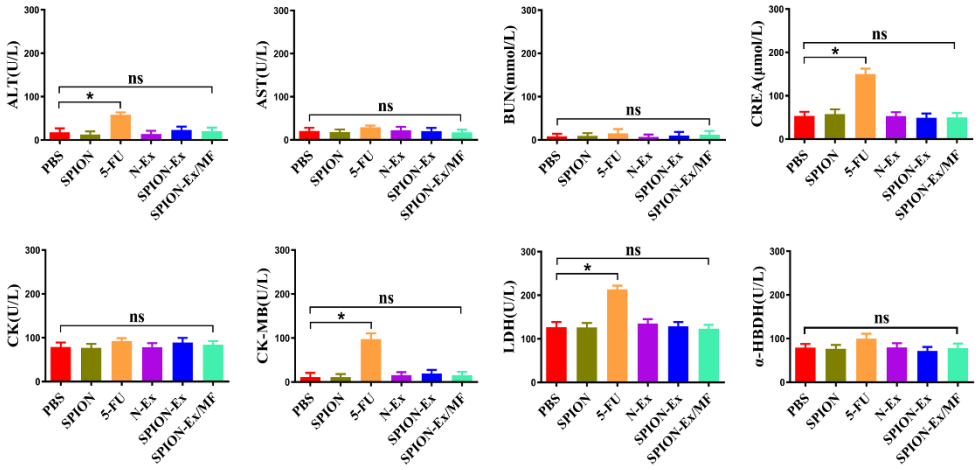

Fig. S22. Blood biochemical tests for mice in different groups.

BALB/c nude mice were sacrificed at three days after last injection of SPION-Ex (day 39) and the blood samples were collected. The expression levels of indicators for liver (ALT and AST), kidney (BUN and CREA) and heart (CK, CK-MB, LDH and α-HBDH) functions were examined by blood biochemical tests. Data are expressed as mean ± SD and analyzed by one-way ANOVA. ns: no significant change, *P< 0.05.

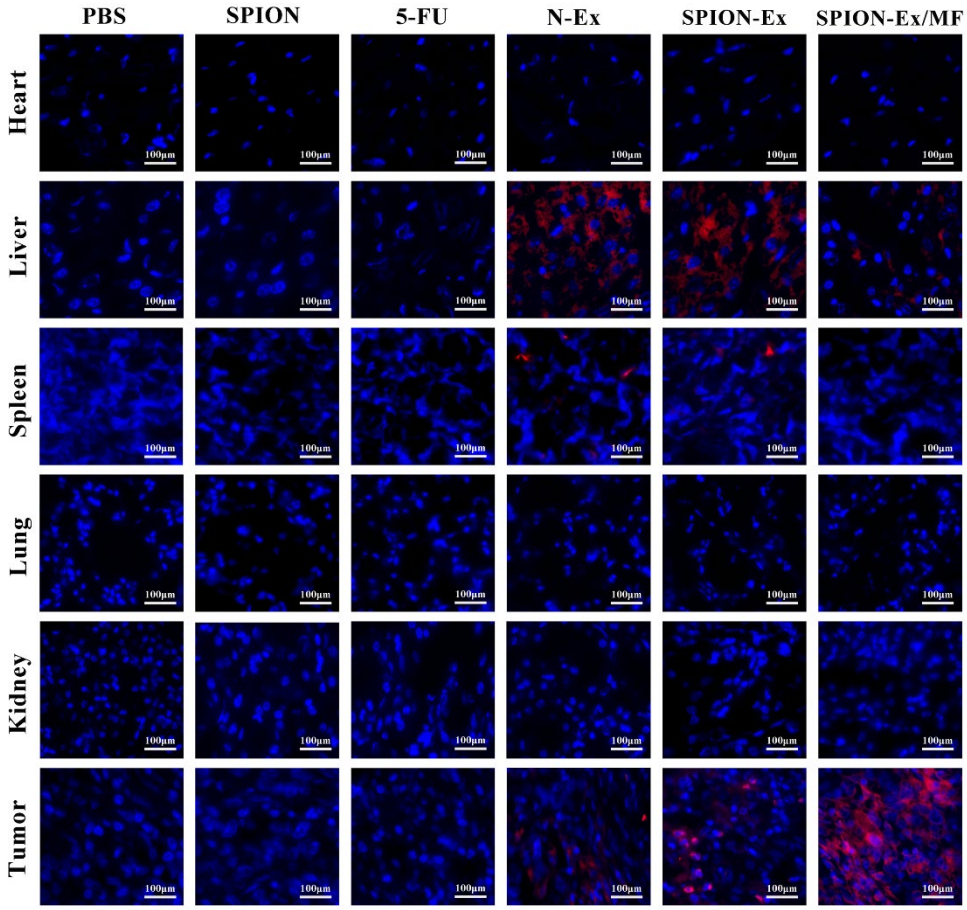

Fig. S23. Increased accumulation of SPION-Ex in mouse tumors under an external MF.

Major organs and tumors of BALB/c nude mice were collected at three days after last injection of SPION-Ex (day 39). SPION-Ex were labeled with DiR (red fluorescence) and cell nuclei were stained with DAPI (blue fluorescence). Scale bar, 100 μm.

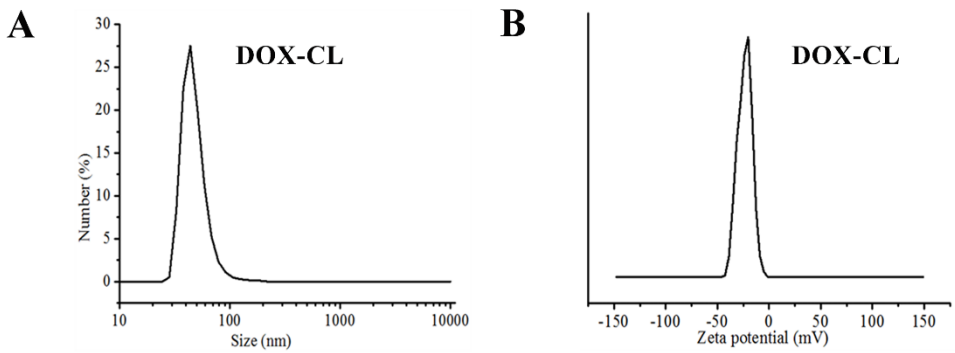

Fig. S24. Size distribution and zeta-potential of DOX-CL.

(**A**) The particle size of DOX-CL assessed by DLS analysis (59±10 nm). (**B**) The zeta-potential of DOX-CL analyzed by DLS (-22±1 mV).

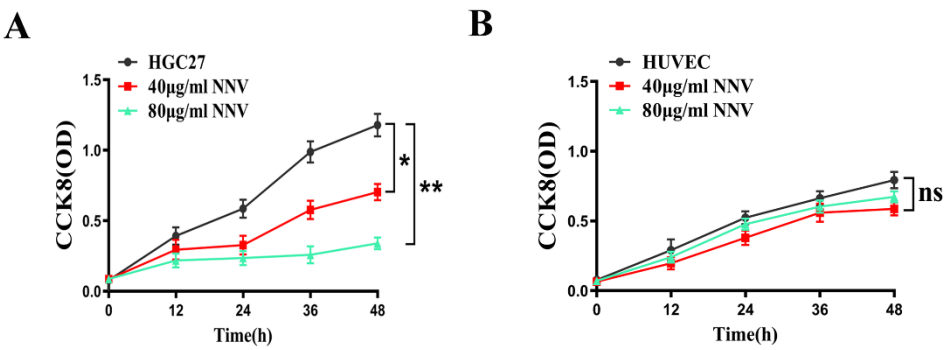

Fig. S25. Cell viability of HGC27 and HUVEC cells treated with NNV.

(**A and B**) Anti-proliferative activity of NNV against HGC27 cells and HUVEC cells. Cells were treated with NNV (0, 40, and 80 μg/mL) for different times (0, 12, 24, 36, and 48 h). Cell viability was determined by CCK-8 assay. Data are expressed as mean ± SD and analyzed by one-way ANOVA. ns: no significant change, **P*< 0.05 and ***P*< 0.01.

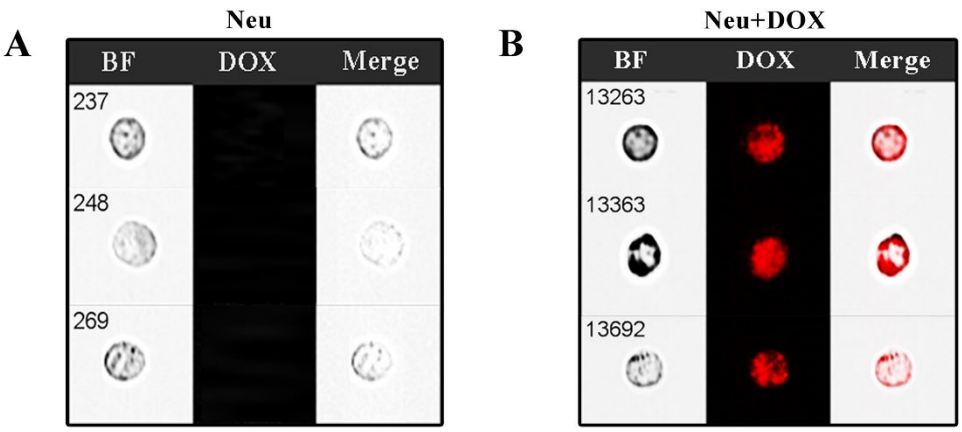

Fig. S26. The uptake of DOX-CL by neutrophils.

(**A and B**) Neutrophils were incubated with DOX-CL at a DOX concentration of 50 μg/ mL and analyzed by imaging flow cytometry.

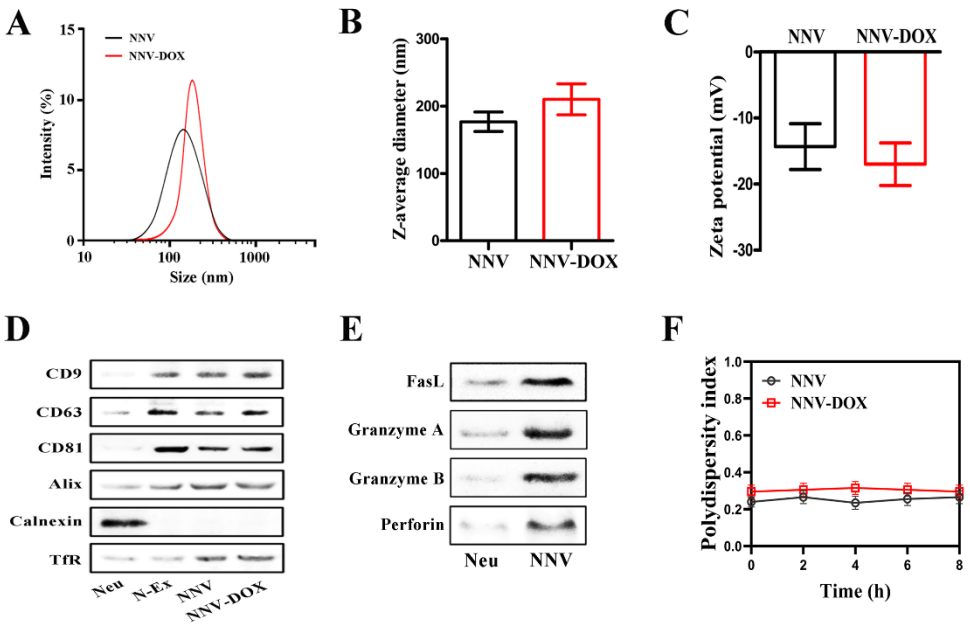

Fig. S27. Characterization of NNV and NNV-DOX.

(**A to C**) Hydrodynamic diameter (**A**), Z-average diameter (**B**), and zeta-potential (**C**) of NNV and NNV-DOX were measured by DLS. (**D**) Western blot analyses of exosomal markers (CD9, CD63, CD81, and Alix), ER marker (calnexin), and TfR in NNV and NNV-DOX. (**E**) The expression of FasL, Granzyme A, Granzyme B, and perforin in NNV was examined by Western blot. Protein lysate from neutrophils (Neu) was used as control. (**F**) The polydispersity indexes of NNV and NNV-DOX at different times were detected by DLS.

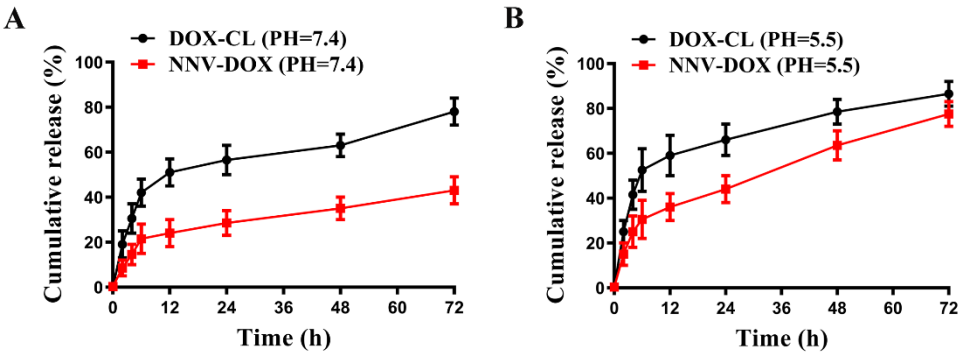

Fig. S28. *In vitro* release profiles of NNV-DOX.

Neutrophils were incubated with DOX-CL (50 μg/mL) and serially extruded for NNV-DOX preparation. (**A and B**) Drug release behaviors of NNV-DOX in PBS buffer (pH=7.4) (A) and acetate buffer (pH=5.5) (B) at indicated times were detected by HPLC. DOX-CL was used as a positive control.

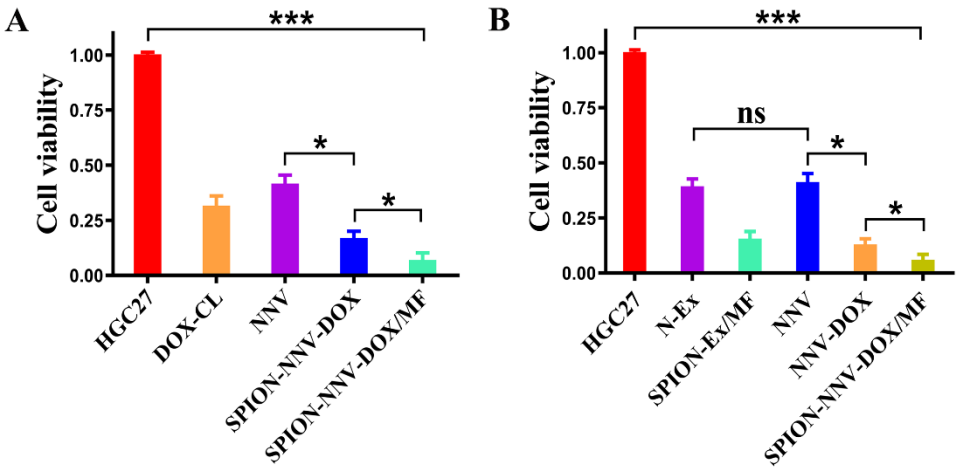

Fig. S29. Effect of SPION-NNV-DOX on tumor cell viability.

(**A**) *In vitro* cytotoxicity of SPION-NNV-DOX (40 μg/mL) to HGC27 cells was evaluated by CCK-8 assay. (**B**) Comparison of the anti-tumor activity between different groups (natural exosomes, SPION modified exosomes, natural nanovesicles, DOX loaded nanovesicles, and targeted DOX-loaded nanovesicles). Data are expressed as mean ± SD and analyzed by one-way ANOVA. *$P < 0.05$, **$P < 0.01$, ***$P < 0.001$.

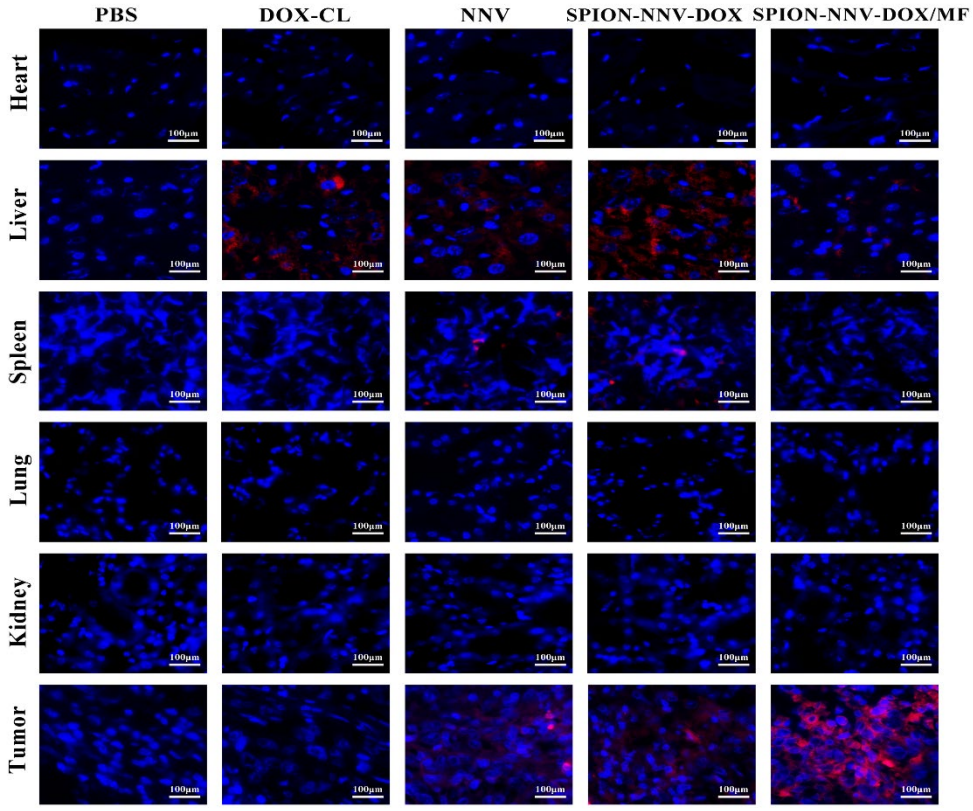

Fig. S30. Distribution of SPION-NNV-DOX in mouse tumors and major organs. Major organs and tumors of BALB/c nude mice were collected at three days after last injection of SPION-NNV-DOX (day 39). Fluorescence intensity (DiR labeled NNV; red fluorescence) in the sections of tumors and major organs were observed by fluorescence confocal laser microscopy. Cell nuclei were stained with DAPI (blue fluorescence). Scale bar, 100 μm.

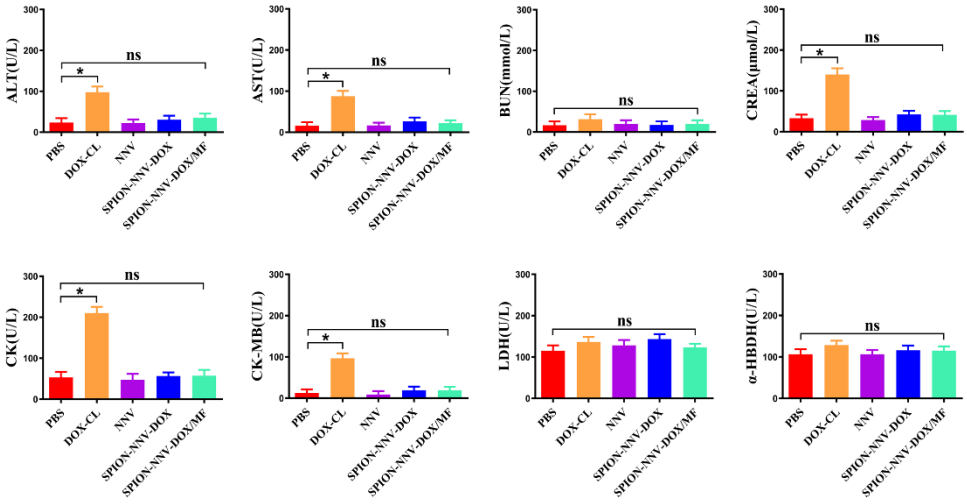

Fig. S31. Blood biochemical tests for mice treated with SPION-NNV-DOX.

BALB/c nude mice were intravenously injected with DOX-CL (5 mg/kg of body weight; 100 μL), NNV (5 mg/kg of body weight; 100 μL), SPION-NNV-DOX (5 mg/kg of body weight; 100 μL) with or without MF. At three days after last injection of SPION-NNV-DOX (day 39), the blood samples were collected and detected by biochemical tests for the expression levels of indicators for liver (ALT and AST), kidney (BUN and CREA) and heart (CK, CK-MB, LDH and α-HBDH) functions. Data are expressed as mean ± SD and analyzed by one-way ANOVA. ns: no significant change, *P< 0.05.

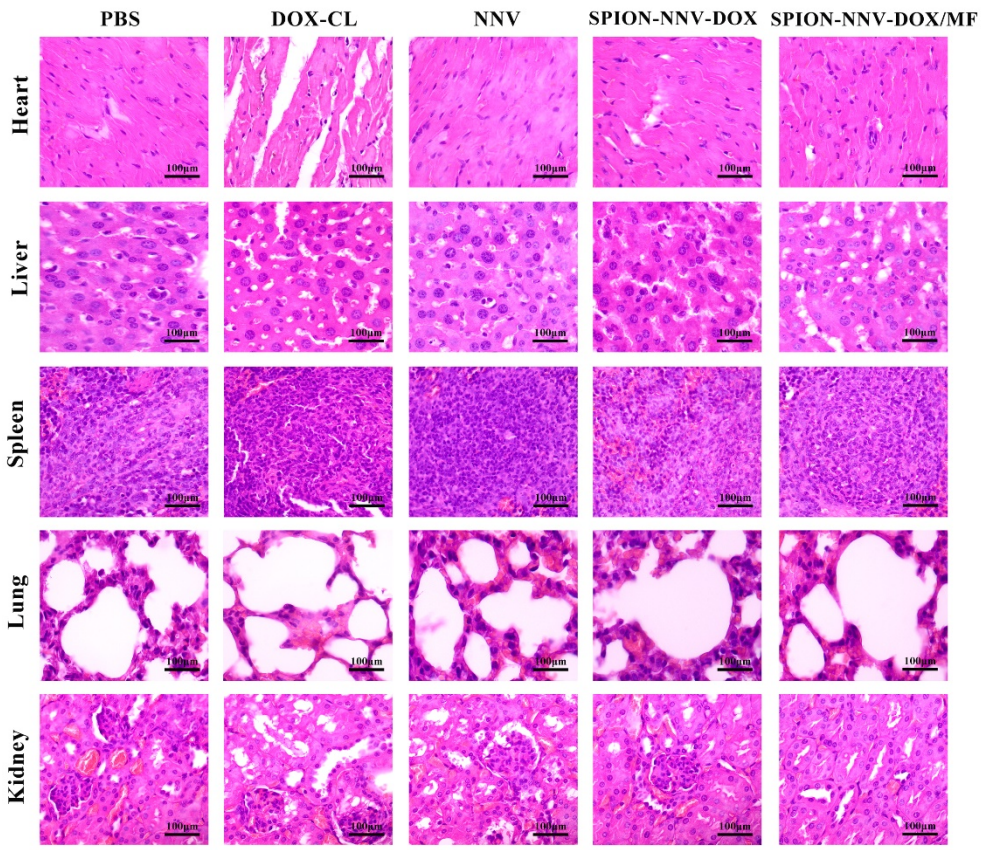

Fig. S32. Safety evaluation of SPION-NNV-DOX in BALB/c nude mice.

Histological analyses of major organs from mice intravenously injected with DOX-CL (5 mg/kg of body weight), NNV (5 mg/kg of body weight), and SPION-NNV-DOX (5 mg/kg of body weight) with or without MF. At three days after last injection (day 39), the major organs (liver, spleen, heart, lung, and kidney) of mice in each group were collected for H&E staining. Scale bar, 100 μm.

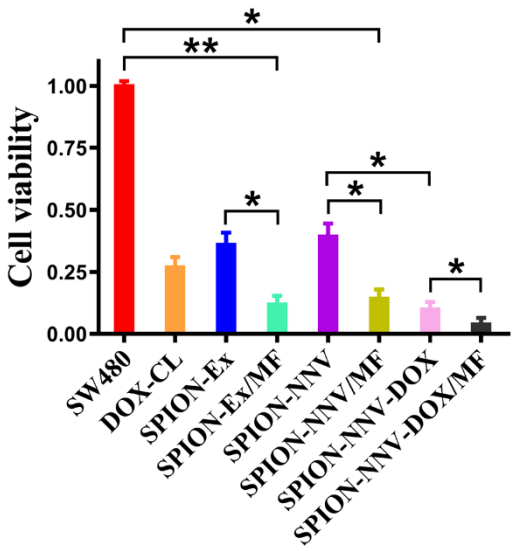

Fig. S33. Improved therapeutic effect of SPION-NNV-DOX than SPION-NNV and DOX-CL alone on tumor cells.

SW480 cells were treated with DOX-CL (45 μg/mL), SPION-Ex (40 μg/mL), SPION-Ex/MF (40 μg/mL), SPION-NNV (40 μg/mL) with or without MF, and SPION-NNV-DOX (40 μg/mL) with or without MF for 24 h. Cell viability was examined by CCK8 assay. Data are expressed as mean ± SD and analyzed by one-way ANOVA. ns: no significant change, $*P < 0.05$, $**P < 0.01$, $***P < 0.001$.

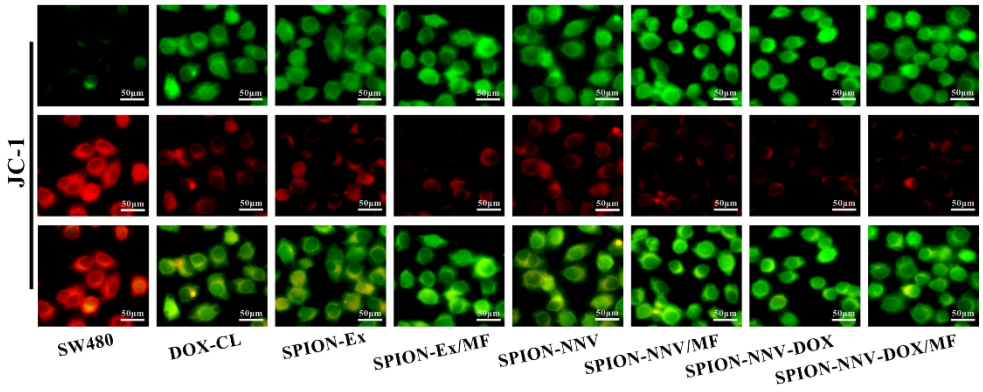

Fig. S34. Mitochondrial membrane potential of tumor cells treated with SPION-NNV-DOX.

SW480 cells were treated with DOX-CL (45 μg/mL), SPION-Ex (40 μg/mL), SPION-Ex/MF (40 μg/mL), SPION-NNV (40 μg/mL) with or without MF, SPION-NNV-DOX (40 μg/mL) with or without MF for 24 h. The mitochondrial membrane potentials of SW480 cells were detected by JC-1 staining. The experiments were performed in triplicate and the representative images were shown. Scale bar, 50 μm.

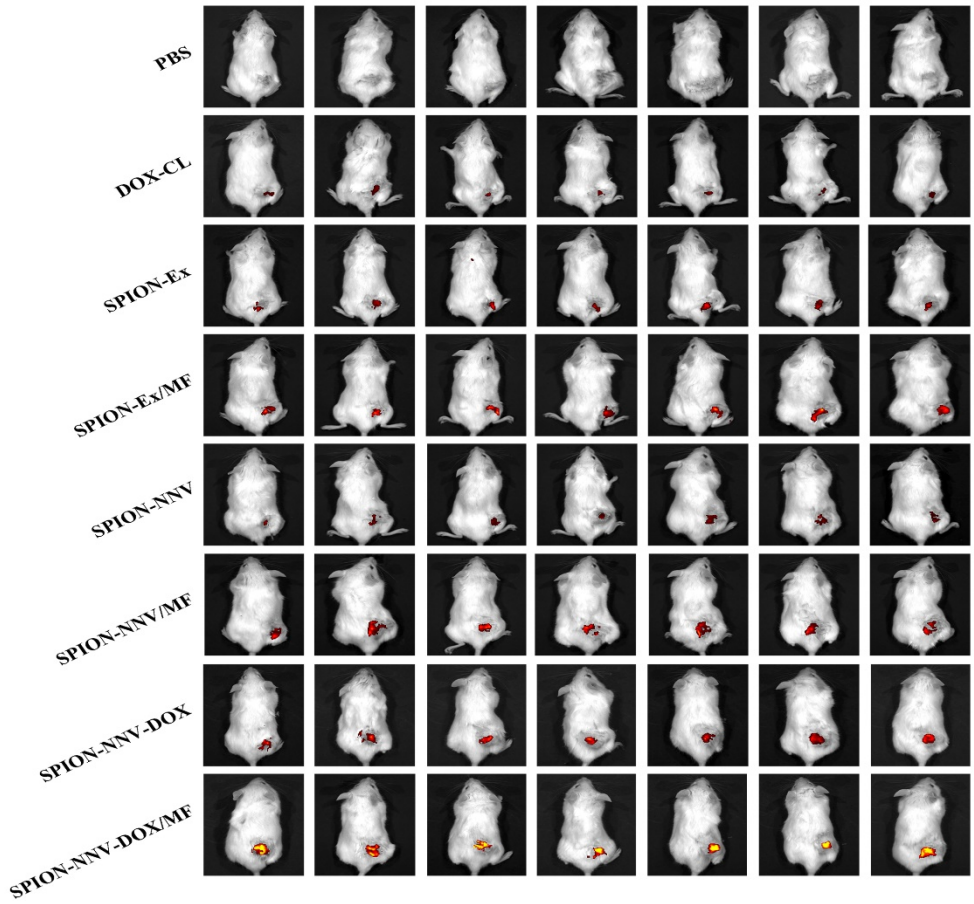

Fig. S35. Distribution of SPION-NNV-DOX in tumors of NCG mice.

NCG mice with SW480 cells-established xenograft tumors were intravenously injected with DOX-CL (5 mg/kg of body weight; 100 μL), SPION-Ex (5 mg/kg of body weight; 100 μL), SPION-NNV (5 mg/kg of body weight; 100 μL), and SPION-NNV-DOX (5 mg/kg of body weight; 100 μL) with or without MF for 7 cycles (4 days per cycle). At three days after the last injection (day 39), the biodistribution of DiR-labeled SPION-Ex, SPION-NNV, and SPION-NNV-DOX was investigated by IVIS imaging system.

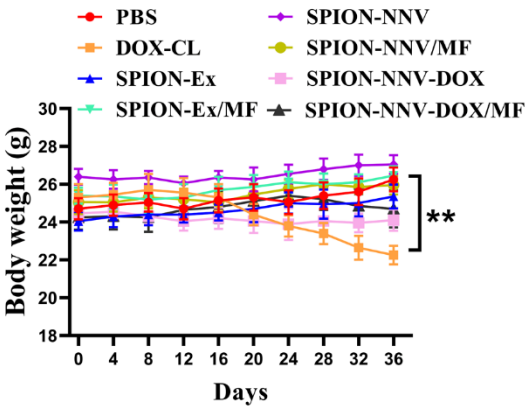

Fig. S36. Body weights of NCG mice in different groups.

Body weights of NCG mice that received different treatments were shown. Data are expressed as mean ± SD and analyzed by one-way ANOVA. **P*<0.05, ***P*<0.01, ****P*< 0.001.

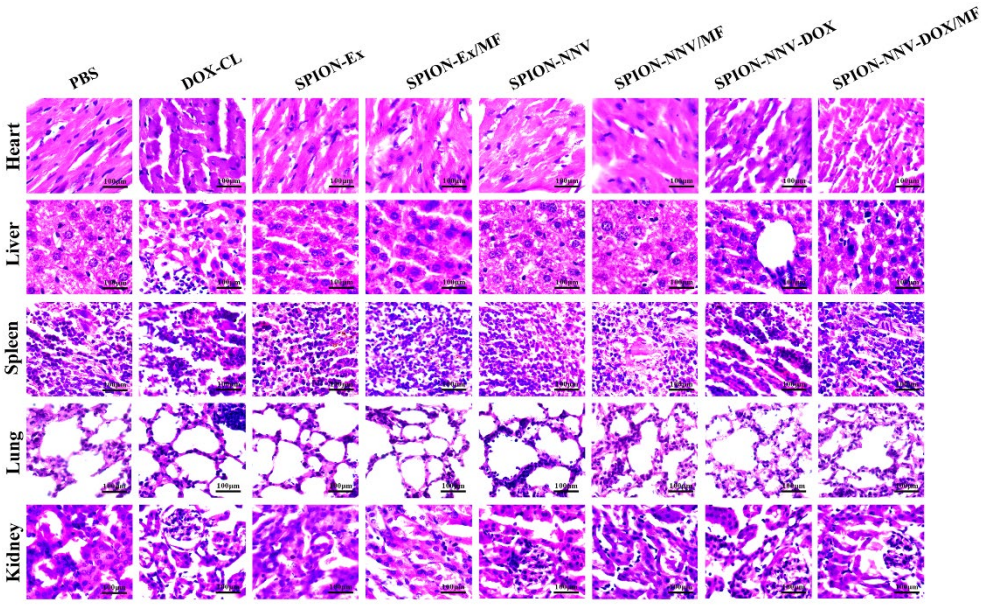

Fig. S37. Histological analyses of major organs in NCG mice.

NCG mice were treated as indicated above. The major organs (heart, liver, spleen, lung, and kidney) of NCG mice in different groups were collected at three days after the last treatment for H&E staining. Scale bar, 100 μm.